Journal of Molecular Structure 1118 (2016) 117–123

Contents lists available at ScienceDirect

Journal of Molecular Structure

journal homepage: http://www.elsevier.com/locate/molstruc

Investigations on surface chemical analysis using X-ray photoelectron spectroscopy and optical properties of Dy^{3+}-doped $LiNa_3P_2O_7$ phosphor

K. Munirathnam [a], G.R. Dillip [b, **], Shivanand Chaurasia [c], S.W. Joo [b, ***], B. Deva Prasad Raju [d, *], N. John Sushma [e]

[a] Department of Physics, Sri Venkateswara University, Tirupati 517 502, India
[b] School of Mechanical Engineering, Yeungnam University, Gyeongsan 712 749, South Korea
[c] High Pressure & Synchrotron Radiation Physics Division, Bhabha Atomic Research Centre, Mumbai 400 085, India
[d] Department of Future Studies, Sri Venkateswara University, Tirupati 517 502, India
[e] Department of Biotechnology, Sri Padmavathi Women's University, Tirupati 517 502, India

ARTICLE INFO

Article history:
Received 13 January 2016
Received in revised form
4 April 2016
Accepted 4 April 2016
Available online 6 April 2016

Keywords:
Pyrophosphate
Solid-state reaction
X-ray photoelectron spectroscopy
White light

ABSTRACT

Near white-light emitting $LiNa_3P_2O_7$:Dy^{3+} phosphors were prepared by a conventional solid-state reaction method. The orthorhombic crystal structure of the phosphors was confirmed using X-ray diffraction (XRD), and the valence states of the surface elements were determined from the binding energies of Li 1s, O 1s, Na 1s, P 2p, and Dy 3d by X-ray photoelectron spectroscopy (XPS). Attenuated total reflectance (ATR) - Fourier transform infrared (FT-IR) spectroscopy was employed to identify the pyrophosphate groups in the phosphors. Diffuse reflectance spectra (DRS) show the absorption bands of the Dy^{3+} ions in the host material. Intense blue (481 nm) and yellow (575 nm) emissions were obtained at an excitation wavelength of 351 nm and are attributed to the $^4F_{9/2} \rightarrow {}^6H_{15/2}$ and $^4F_{9/2} \rightarrow {}^6H_{13/2}$ transitions of Dy^{3+} ions, respectively. The combination of these two intense bands generates light emission in the near-white region of the chromaticity diagram.

1. Introduction

Over the past few years, there has been increasing demand for luminescent materials for a wide range of applications, including plasma display panels (PDPs), Hg-free lamps, liquid crystal display (LCD) backlights, and quickly commercializing solid-state lighting (SSL) sources [1,2]. SSL devices have several advantages for lighting like significant power savings, longer lifetime, higher luminous efficiency, and environmental friendliness compared to conventional incandescent or fluorescent lamps [3].

Phosphor-converted light-emitting diodes (pc-LEDs) have received great attention due to their stable color, good color reproducibility, and higher color rendering indexes compared to RGB (red, green, and blue) LEDs. SSL devices based on pc-LEDs are commercializing quickly, but they suffer from various disadvantages like a poor color-rendering index (CRI) and low stability of the color temperature (CCT) [4–6]. To overcome these weaknesses, researchers have made numerous efforts to develop single-phase phosphors for white light generation. Various approaches are used to obtain white light emission in a single-phase host. The four following approaches are mainly considered for single-host white-emitting phosphors [3,7]: (i) introducing a suitable rare-earth (RE) ion (Eu^{3+}, Dy^{3+}, etc.) into the appropriate single-phase host matrix [8,9]; (ii) combining different RE ions (Tm^{3+}/Dy^{3+}, Eu^{2+}/Tb^{3+}/Mn^{2+}, etc.) with various emissions (red, green, blue, or yellow) [10,11]; (iii) selective co-doping of ion pairs ($Ce^{3+} \rightarrow Mn^{2+}$, $Eu^{2+} \rightarrow Mn^{2+}$, etc.) via an energy transfer mechanism [12,13]; and (iv) inducing appropriate defects in the luminescent materials (defect-related emissions) [14].

A suitable host matrix and dopant ion is important for obtaining a single-phase white-lighting phosphor. Phosphate-based phosphors are an important family of luminescent materials because of their excellent properties, such as a large band gap, high absorption

* Corresponding author.
** Corresponding author.
*** Corresponding author.
E-mail addresses: dillip.ngr@gmail.com (G.R. Dillip), swjoo@yu.ac.kr (S.W. Joo), drdevaprasadraju@gmail.com (B. Deva Prasad Raju).

http://dx.doi.org/10.1016/j.molstruc.2016.04.004
0022-2860/

of PO_4^{3-} in the UV region (300–400 nm), cheaper raw materials, simple synthesis conditions, high thermal and chemical stability, and exceptional optical damage threshold [9,15]. Phosphate-based phosphors are a good host matrix for RE ion transitions. The interaction between the RE ions is weak in these matrices because the RE ions are separated from each other by the phosphate groups [16]. Therefore, one can expect good optical properties from these materials.

Among the various lanthanide ions, trivalent dysprosium ions (Dy^{3+}) have attracted significant attention since dysprosium-doped phosphors can be used in fluorescent lamps as a tricolor component and single-phase full-color phosphor in pc-LEDs [17]. Under n-UV excitation, there are generally three consistent bands in the visible region, including blue (470–500 nm), yellow (570–600 nm), and feeble red (670 nm) emissions, which are achieved when Dy^{3+} ions are incorporated in wide-band-gap host materials. These bands are associated with the hypersensitive electric dipole (ED) $^4F_{9/2} \rightarrow {}^6H_{15/2,\,13/2}$ transition and optical $^4F_{9/2} \rightarrow {}^6H_{11/2}$ transition in Dy^{3+} ions [18,19].

One strategy to achieve white light emission is adjusting the ratio of yellow to blue emission intensity, which reflects the coordination surroundings of the Dy^{3+} ion. Doping Dy^{3+} into an appropriate host is another strategy to obtain potential candidates for industrial applications [20]. In the present work, a simple and inexpensive phosphate host matrix and a suitable single RE dopant (Dy^{3+}) ion were investigated for their suitability in single-phase emission in the white light region. To the best of our knowledge, the optical properties of $LiNa_{3-x}P_2O_7$: xDy^{3+} phosphor has not been reported previously. The surface chemical composition of the elements in the phosphors was studied in detail by X-ray photoelectron spectroscopy.

2. Experimental

2.1. Synthesis

Polycrystalline powders of $LiNa_{3-x}Dy_xP_2O_7$ (x = 0, 0.05, 0.07, 0.09, and 0.11) were prepared by a solid-state reaction method. The materials were synthesized using the same experimental conditions as those in a recently published study [21]. In brief, analytical reagent-grade high-purity (99.99%) starting materials of Li_2CO_3, Na_2CO_3, $NH_4H_2PO_4$, and Dy_2O_3 were purchased (Sigma–Aldrich, USA) and used without further purification. To obtain homogeneity, stoichiometric amounts of reactive mixtures were finely ground in an agate mortar for 1 h. Each of the mixtures was placed in a separate silica crucible and gradually heated in a muffle furnace from room temperature (RT) to 400 °C for 4 h. This process eliminates the residual water, CO_2, and NH_3 from the mixtures. The samples were re-ground after cooling down to RT and then sintered at 540 °C for 12 h with several intermediate grindings. Finally, the samples were furnace cooled, ground again, and used for characterization.

2.2. Characterization

X-ray diffraction (XRD) patterns were collected using an X-ray diffractometer (PANalytical X'Pert PRO, USA) in a 2θ range of 10 to 70° with *Cu* K_α radiation at a wavelength of $\lambda = 1.5405$ Å. Attenuated total reflectance (ATR) - Fourier transform infrared (FTIR) spectra were recorded in the wavenumber range of 4000 to 400 cm^{-1} on a Perkin–Elmer (Bruker) IR spectrometer.

X-ray photoelectron spectroscopy (XPS) analysis was performed on an X-ray photoelectron spectrometer (K-alpha, Thermo Scientific, USA) using *Al* K_α X-ray radiation (1486.6 eV). All experiments were performed at analyzing chamber pressure of 1.8×10^{-8} mbar using pass energies of 160 and 30 eV and step sizes of 1 eV and 0.1 eV for the low and high-resolution spectra, respectively. Prior to measurements, the XPS instrument work function was calibrated with the standard Au $4f_{7/2}$ metallic binding energy (83.9 eV) and the spectrometer dispersion is adjusted to metallic Cu $2p_{3/2}$ binding energy (932.6 eV). The data were recorded and processed using the commercial software Avantage (Version 5.932, Thermo Scientific, USA). The charge shift corrections of the binding energies were adjusted relative to the carbon (C 1s = 284.8 eV) from hydrocarbons adsorbed on the surface of sample. Each core level spectrum was first fitted with a Shirley-type background and then deconvoluted into various components using GL30 (a mixture of Gaussian (70%) and Lorentzian (30%)) in Avantage. In the process of deconvolution of a signal, the full-width at half-maximum (FWHM) of each elemental spectrum was kept at similar value for different contributions.

The morphology of the sample was analyzed using a field-emission scanning electron microscope (FE-SEM) (S-4200, Hitachi, Japan). UV–Vis diffuse reflectance spectra (DRS) were recorded on a UV–Vis–NIR spectrophotometer (Jobin Varian Cary 5000, USA). The reflectance was measured in the range of 800 to 200 nm using polytetrafluoroethylene (PTFE) as a standard. Photoluminescence (PL) emission and excitation (PLE) spectra were recorded using a fluorescence spectrophotometer (Jobin Vyon Fluorolog–3, USA) with a xenon lamp as an excitation source. All the measurements were recorded at RT.

3. Results and discussion

3.1. X-ray diffraction analysis

The phase purity of the prepared pyrophosphate $LiNa_3P_2O_7$:Dy^{3+} phosphors were characterized by powder XRD analysis. The XRD patterns of the Dy-doped $LiNa_3P_2O_7$ samples are shown in Fig. 1. The dominant reflections of all the samples were well indexed with the host structure ($LiNa_3P_2O_7$) recently reported by Shi et al. [22] as well as the Inorganic Crystal Structure Data (ICSD: 424375). There were no other impurities in the patterns, indicating purity of the synthesized powders.

A closer look at the figure indicates that the predominant XRD peak positions are shifted toward a higher 2θ angle with increasing dopant concentration. In general, distortion of the XRD peaks from their mean position could be influenced by many factors, such as

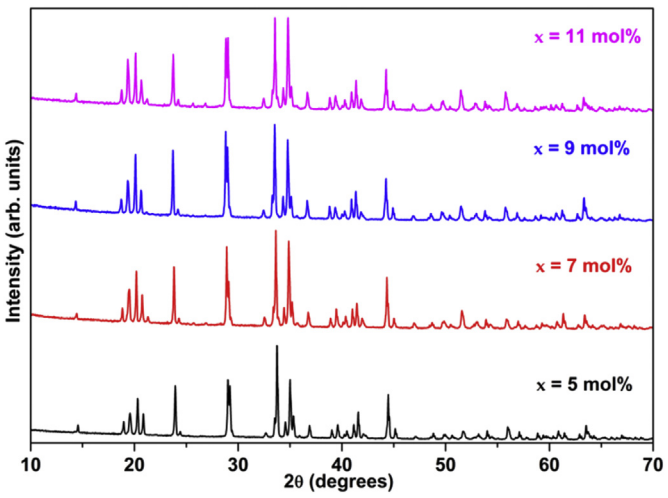

Fig. 1. XRD patterns of $LiNa_3P_2O_7$:Dy^{3+} phosphor (Dy^{3+} = 5–11 mol%).

the annealing temperature [23], the addition of impurities [24], and the synthesis method [25]. In the present case, the samples were prepared by solid-state reaction method in air by adding impurities to the host lattice in the same experimental conditions. Therefore, the temperature and synthesis method were discarded as influential factors. The peak shifting could be due to the addition of Dy^{3+} ions to the host structure. The added impurity ions would substitute at the host cation sites.

The ionic radii of Li^{+}, Na^{+}, P^{5+}, and Dy^{3+} are 0.059 nm (coordination number (CN) = 4), 0.118 nm (CN = 8), 0.017 nm (CN = 4), and 0.103 nm (CN = 8), respectively [26–28]. Because of the similar ionic radii of the host cations, the Dy^{3+} ions occupy the Na^{+} ion sites in the host structure. These results in the slight XRD peak shifting of the samples to a higher two-theta angle as a function of the dopant concentration because of the difference in ionic radii.

3.2. FTIR spectral studies

FTIR spectra of $LiNa_3P_2O_7:Dy^{3+}$ phosphors (Dy^{3+} = 5–7 mol%) are shown in Fig. 2. For all samples, the spectra have similar profiles without any other phases, suggesting that the variation of Dy concentration did not have much effect on the structure of the host. The two peaks at 747 and 911 cm^{-1} are due to the symmetric and asymmetric vibrational stretching modes of P–O–P bridges [29]. The small peak at 1633 cm^{-1} corresponds to the stretching vibration of PO_4^{3-} groups, which revealed that the phosphors have the molecular structure of pyrophosphates. The absorption peaks showed good agreement with those reported for the $LiNa_3P_2O_7$ host compound [22,29]. Peaks are negligible or non-existent in the range of 3655–3535 cm^{-1}, which indicates the absence of water molecules (–OH) in the samples [19]. The identified band assignments confirmed the presence of diphosphate groups in the $LiNa_3P_2O_7:Dy^{3+}$ phosphors.

3.3. XPS studies

X-ray photoelectron spectroscopy was employed to ascertain the chemical composition, electronic state, and binding energies of the prepared phosphor. A survey scan of 5 mol% Dy^{3+}-doped $LiNa_3P_2O_7$ phosphor was recorded in the range of 1350 to 0 eV, as shown in Fig. 3 (a). The peaks at around 55, 531, 1071, 133, and 1296 eV correspond to the Li 1s, O 1s, Na 1s, P 2p, and Dy 3d levels, respectively. No other impurity peaks were identified in the spectrum, which supports the XRD and FTIR analyses.

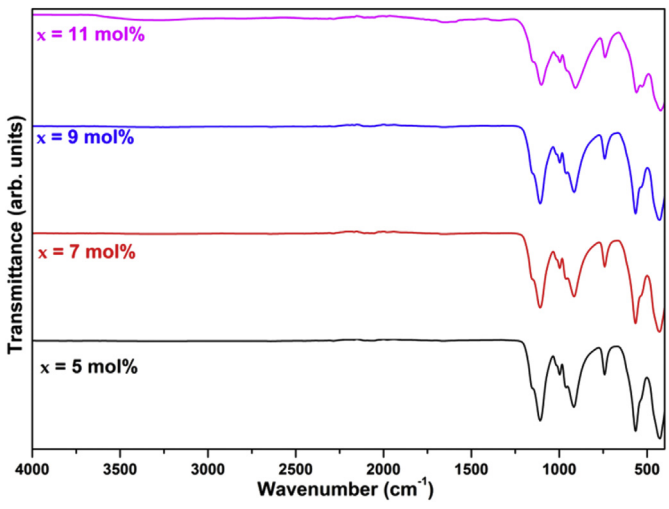

Fig. 2. FTIR spectra of $LiNa_3P_2O_7:Dy^{3+}$ phosphor (Dy^{3+} = 5–11 mol%).

To study the bonding information in detail, high-resolution spectra of Li 1s, O 1s, Na 1s, P 2p, and Dy 3d were measured, as shown in Fig. 3 (b)–(f), respectively. All the core-level spectra were further deconvoluted into various sub-components using a GL30 program. As shown in Fig. 3 (b), the signal to noise (S/N) ratio of the Li 1s is very low. This results from the low X-ray scattering factor and limited sensitivity of the XPS technique for detecting light elements like lithium. The Li 1s spectrum was fitted to a single broad peak, suggesting that the only one type of bonding is possible in the present compound. The peak centered at about 55.0 eV corresponds to the oxygen-coordinated lithium atom (Li–O) in $LiNa_3P_2O_7:Dy^{3+}$ phosphor, which also suggests that the Li atoms are in the normal oxidation state (Li^{+}). This is consistent with the binding energy of Li in LiOH and Li_2CO_3 compounds [30–32].

The O 1s spectrum was deconvoluted into five peaks that are attributed to the various bonding of oxygen in the $LiNa_3P_2O_7:Dy^{3+}$ phosphor. The different contributions are decomposed by keeping same FWHM for lower binding energies (O1 to O4 peaks) and different value for the latter higher binding energy contribution (O5 (535.4 eV)), which is presented in Table 1. This is because of sodium Auger overlap with the O 1s. The O1s peaks at O1, O2 and O3 are arising from oxygen atoms existing in various structural bonds of phosphor: P–O–P, P–O–Li and P–O–Na. According to Pauling, the electronegativity of Phosphorous, Lithium and Sodium are 2.19, 0.98 and 0.93, respectively. Therefore, the O1 (530.8 eV) is assigned to P–O–P pyrophosphates (or double bond P=O), while the other two O2 (531.5 eV) and O3 (532.5 eV) are attributed to the P–O–Li and P–O–Na (or partially from Dy–O) structural bonds, respectively. The O4 peak at 533.4 eV is due to the OH^{-} and oxygen in H_2O, which are adsorbed on the sample surface during the preparation of sample for analysis in non-vacuum condition [31,33–38].

The P 2p core level spectrum is composed of two symmetrical peaks of phosphorus doublets (P $2p_{3/2}$ and $2p_{1/2}$) at P1 (133.5 eV) and P2 (134.6 eV). The binding energy difference between the P $2p_{3/2}$ and $2p_{1/2}$ core levels was 1.1 eV with a ratio of ~0.5, which is comparable with the literature value (1 eV) [37]. As reported in the crystal structure of $LiNa_3P_2O_7$ [22], the various bonds are possible with oxygen in the phosphor: P–O–P and P–O–Li (or Na). This leads to difference in binding energies of P 2p peak. Therefore, the higher binding energy peak corresponds to phosphorus in the pyrophosphate groups, P–O–P (or double bond P=O), while latter binding energy peak is owing to the phosphorous in the bond P–O–Li (or Na) (according to Pauling electronegativity of the elements) [33,37,38]. The similar bonds are also observed in the O 1s spectrum (Table 1).

The Dy 3d spectrum was fitted to a single peak near 1296.6 eV, which is assigned to the Dy–O bond of Dy $3d_{5/2}$ [35]. The intensity of the spectrum (Fig. 3 (f)) is lower because of the lower dopant concentration in the phosphor. The fitted elemental percentage of the $LiNa_3P_2O_7:Dy^{3+}$ phosphor (Dy^{3+} = 5 mol%) is presented in Table 1.

3.4. Morphological studies

To investigate the surface morphology of the synthesized phosphor, SEM micrographs were recorded by field emission scanning electron microscope (FE-SEM). A typical SEM image of $LiNa_3P_2O_7:Dy^{3+}$ phosphor (Dy^{3+} = 9 mol%) is represented in Fig. 4. The phosphor has irregular morphology due to the calcination of the samples at high temperature and intermediate grinding between the calcinations. The particles are formed by several rock-like structures with non-uniform sizes and shapes. A closer look indicates that the grains vary in size from a few microns to several tens of microns.

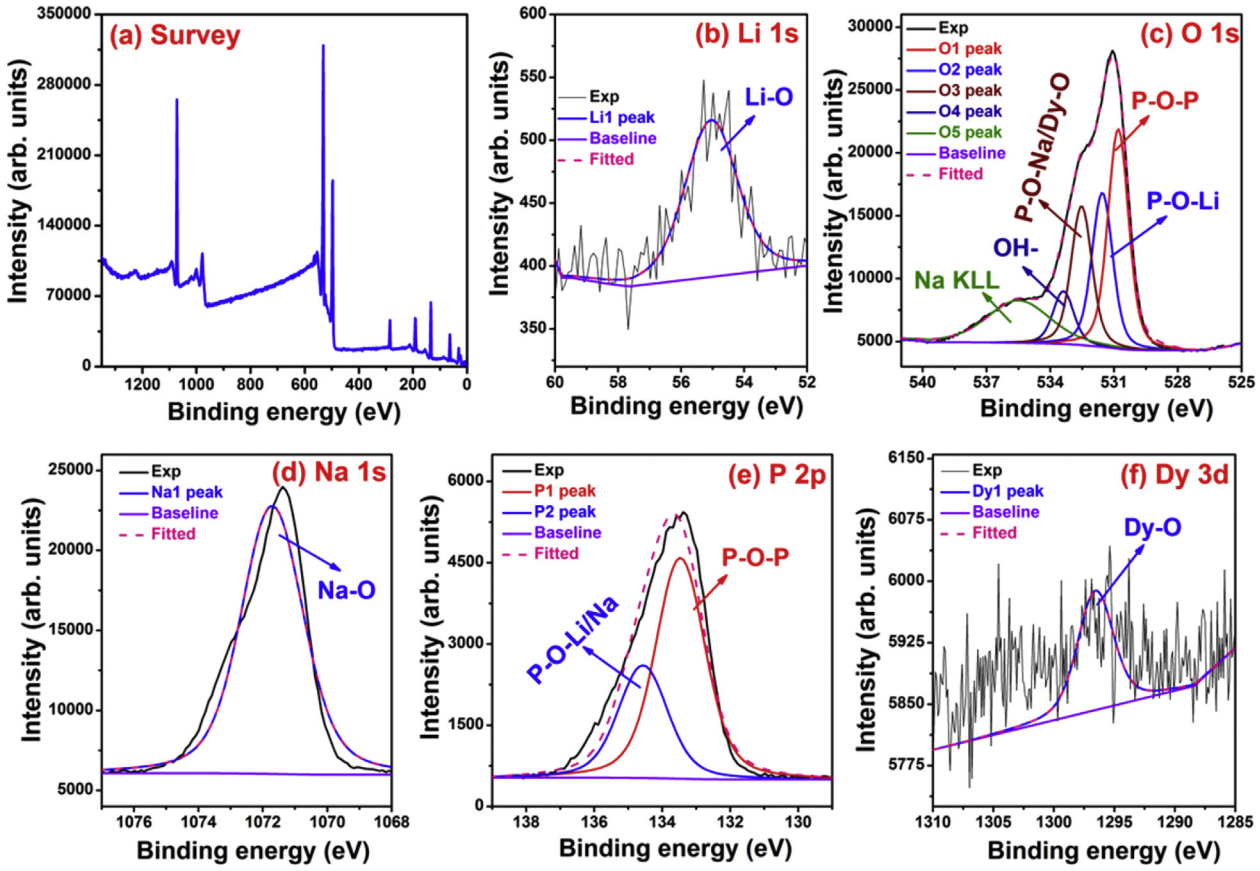

Fig. 3. High (a) and low resolution scans of Li 1s (**b**), O 1s (**c**), Na 1s (**d**), P 2p (**e**), and Dy 3d (**f**) of the $LiNa_3P_2O_7:Dy^{3+}$ phosphor (Dy^{3+} = 5 mol%).

Table 1
Peak binding energy, FWHM, area and atomic percentage from the curve fitting of core-level spectra of elements, Li 1s, O 1s, Na 1s, P 2p, and Dy 3d for $LiNa_3P_2O_7:Dy^{3+}$ (Dy^{3+} = 5 mol%) phosphor. The uncertainty in the peak position and FWHM are ±0.1 eV.

Region	Peak	Peak binding energy (eV)	FWHM (eV)	Area	Relative at%	Elemental at%	Assignment
Li 1s	Li1	55.0	1.96	286.8	7.84	7.84	Li–O
O 1s	O1	530.8	1.15	23556.4	18.59	58.74	P–O–P
	O2	531.5	1.15	16533.9	13.05		P–O–Li
	O3	532.5	1.15	14897.7	11.77		P–O–Na/Dy–O
	O4	533.4	1.15	5650.2	4.46		Chemisorbed OH^-
	O5	535.4	3.48	13722.1	10.87		Na KLL Auger line
Na 1s	Na1	1071.7	2.27	44517.4	17.44	17.44	Na–O
P 2p	P1	133.5	1.72	8189.9	15.93	15.93	P–O–P
	P2	134.6	1.72	4183.2			P–O–Li (or Na)
Dy 3d	Dy1	1296.6	3.50	598.4	0.05	0.05	Dy–O

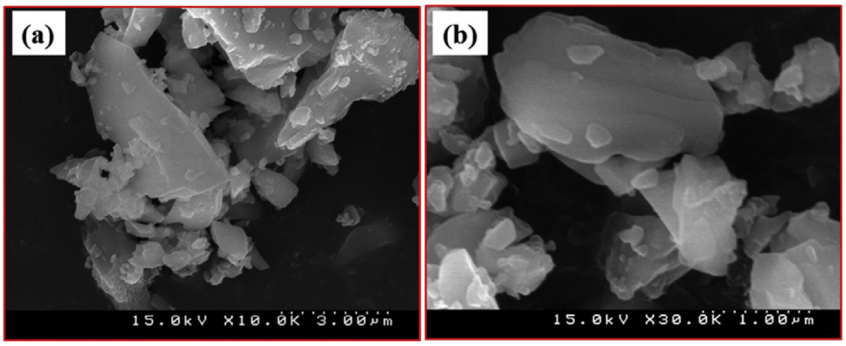

Fig. 4. Low-magnification (**a**) and high-magnification (**b**) SEM images of $LiNa_3P_2O_7:Dy^{3+}$ phosphor (Dy^{3+} = 9 mol%).

3.5. Diffuse reflection spectra (DRS)

Diffuse reflection spectra were recorded to investigate absorption properties of the samples, as shown in Fig. 5. There is a broad absorption band in the range of 250–320 nm due to the charge transition (CT) band in the host [22]. The other absorption bands at 326 nm ($^6H_{15/2} \rightarrow {}^4L_{19/2}$), 352 nm ($^6H_{15/2} \rightarrow {}^4I_{11/2}$), 366 nm ($^6H_{15/2} \rightarrow {}^6P_{7/2}$), and 388 nm ($^6H_{15/2} \rightarrow {}^4I_{13/2}$) are due to *f–f* transitions of Dy^{3+} ions in the phosphor [19,39]. With the increase of Dy concentration, all the absorption peaks related to *f–f* transitions of Dy^{3+} ions also increased. The peak at about 352 nm is the predominant peak, suggesting suitability of the phosphors for n-UV excitation applications. The prepared samples have very good absorption in the range of 250–320 nm due to the presence of PO_4^{3-} groups, which supports the FT-IR analysis.

3.6. Photoluminescence properties

The excitation spectra of $LiNa_3P_2O_7:Dy^{3+}$ phosphors are shown in Fig. 6. In the range of 300–500 nm, the excitation spectra consist of a series of characteristic bands that are attributed to the transitions of $^6H_{15/2} \rightarrow {}^4L_{19/2}$ (328 nm), $^6H_{15/2} \rightarrow {}^6P_{7/2}$ (351 nm), $^6H_{15/2} \rightarrow {}^6P_{5/2}$ (367 nm), $^6H_{15/2} \rightarrow {}^4I_{13/2}$ (388 nm), $^6H_{15/2} \rightarrow {}^4F_{7/2}$ (395 nm), $^6H_{15/2} \rightarrow {}^4G_{11/2}$ (427 nm), $^6H_{15/2} \rightarrow {}^4I_{15/2}$ (453 nm), and $^6H_{15/2} \rightarrow {}^4F_{9/2}$ (471 nm), respectively [9,40]. The band at 351 nm is the predominant peak and was used for further emission spectra measurements. The excitation peaks were consistent with the bands from DRS analysis. The excitation spectra reveal that Dy^{3+} ions could be excited effectively by n-UV sources with a wavelength of 351 nm, offering new potential for white-light phosphors.

The photoluminescence emission spectra were measured under excitation at 351 nm, as shown in Fig. 7. There were two strong characteristic peaks centered at 485 nm (blue) and 575 nm (yellow). These bands correspond to the MD $^4F_{9/2} \rightarrow {}^6H_{15/2}$ transition and the ED $^4F_{9/2} \rightarrow {}^6H_{13/2}$ transition, respectively [17,18]. The transitions of ions in the dopant (Dy^{3+}) in excitation and emission states are clearly presented in the energy level diagram shown in Fig. 8.

To optimize the critical dopant concentration, the Dy^{3+} ion dopant concentration in the host was varied (as described in the experimental section). With increased dopant concentration in the host, the emission spectra appear to have similar profiles with the same peak positions of peaks but with variations in their relative intensity. The intensity of the emission peaks increased with the dopant concentration from 5 to 9 mol%, beyond which the intensity decreased due to the concentration quenching effect. In many inorganic materials, the luminescence intensity remarkably decreases because of non-radiative transition between the similar dopant Dy^{3+} ions before being emitted to the ground level and reduction in the average distance between Dy^{3+}, which leads to the quenching effect [41]. The emission spectra show that the blue emission peak at 485 nm due to the magnetic transition ($^4F_{9/2} \rightarrow {}^6H_{15/2}$) dominates over the yellow emission peak at 575 nm due to electric transition ($^4F_{9/2} \rightarrow {}^6H_{13/2}$). This illustrates that Dy^{3+} ions occupied the high-symmetry sites with inversion centers in the host matrix [42].

Further information can be revealed by calculating the asymmetric ratio, which is the ratio of the luminescence intensities due to ED transition and MD transition. The relative intensity ratio of the yellow (575 nm) to blue (481 nm) emission can be used to analyze the structural distortion around Dy^{3+} ions: $(R) = I_e$ ($^4F_{9/}$

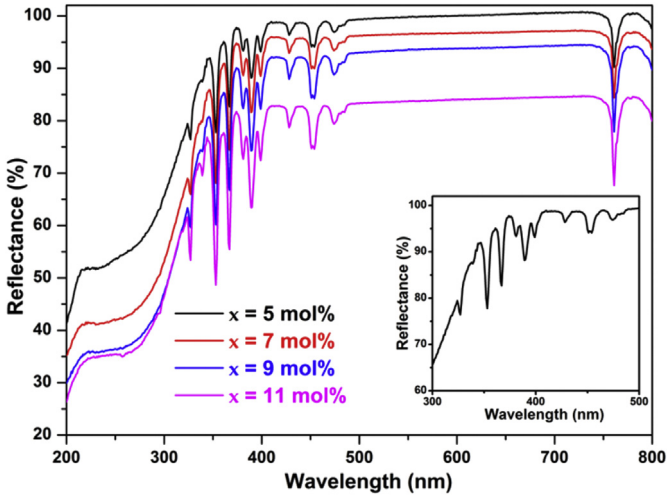

Fig. 5. DRS of $LiNa_3P_2O_7:Dy^{3+}$ phosphor (Dy^{3+} = 5–11 mol%). Inset shows the magnified view of DRS of $LiNa_3P_2O_7:Dy^{3+}$ phosphor (Dy^{3+} = 5 mol%) between 300 and 500 nm.

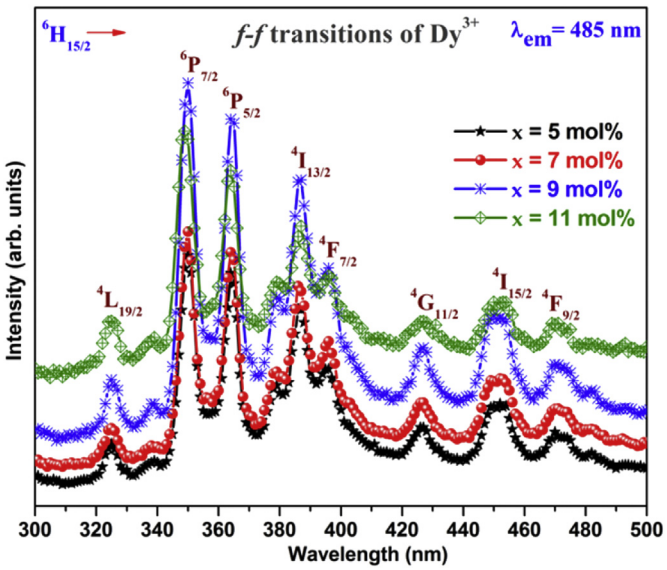

Fig. 6. Excitation spectra of $LiNa_3P_2O_7:Dy^{3+}$ phosphor (Dy^{3+} = 5–11 mol%).

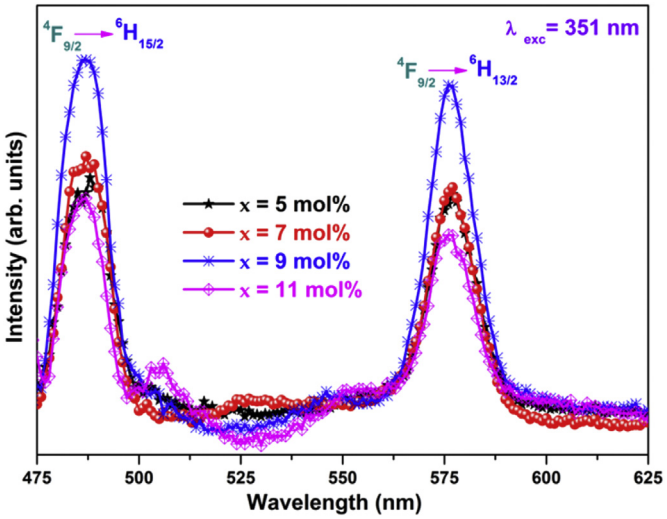

Fig. 7. Emission spectra of $LiNa_3P_2O_7:Dy^{3+}$ phosphor (Dy^{3+} = 5–11 mol%).

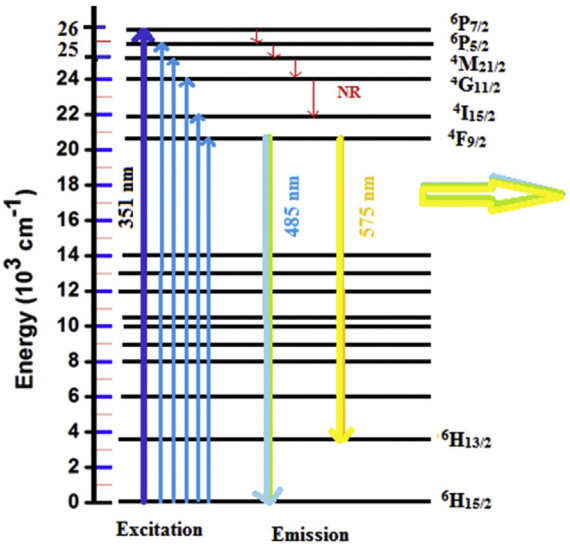

Fig. 8. Energy level diagram of *f–f* transitions of Dy^{3+} ions in $LiNa_3P_2O_7$ host.

$_2 \rightarrow {}^6H_{13/2})/I_m$ ($^4F_{9/2} \rightarrow {}^6H_{15/2}$) [39]. The *R* values were found to be 0.87, 0.88, 0.93, and 0.83 for $LiNa_3P_2O_7:Dy^{3+}$ (Dy^{3+} = 0.05, 0.07, 0.09, and 0.11), respectively. These values indicate that the ratio increased with increasing Dy^{3+} ion concentration from 0.87 to 0.93 and then decreased thereafter. Lower *R* values lead to higher symmetry of the dopant ions at the host cation sites, and since the obtained *R* values were small, it can be concluded that Dy^{3+} ions occupy high-symmetry sites [43].

3.7. CIE parameters

The *x* and *y* values of the 1931 CIE chromaticity coordinates of the $LiNa_3P_2O_7:Dy^{3+}$ phosphor (Dy^{3+} = 9 mol%) were calculated using color coordinate calculation software and are presented in Fig. 9. CIE values of the phosphor were calculated in three regions of the emission spectra. The color coordinates are *a* ((0.103, 0.127); 461–500 nm), *b* ((0.469, 0.501); 560–600 nm), and *c* ((0.281, 0.338); 461–650 nm). These CIE values are located in the blue, yellow, and near-white regions, respectively (see Fig. 9).

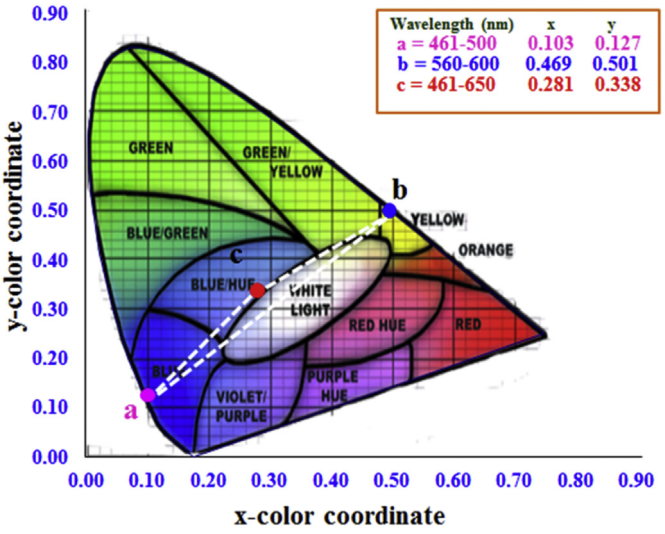

Fig. 9. CIE diagram of $LiNa_3P_2O_7:Dy^{3+}$ phosphor (Dy^{3+} = 9 mol%).

The white dotted lines in the figure show that a suitable combination of the blue and yellow emission will produce white light emission. It is known that suitable ratios of yellow to blue (Y/B) emissions could produce white light in single-phase host materials. By varying the Dy concentration in the host matrix, the Y/B ratios could also vary. The Y/B value is equal to unity at a particular concentration, which is one of the significant criteria for obtaining white light in Dy-doped phosphors. Similar results were published previously [19]. However, in the present case, the Y/B ratio is 0.93 for 9 mol%, which produces near-white light.

4. Conclusions

$LiNa_3P_2O_7:Dy^{3+}$ phosphors (Dy^{3+} = 5–11 mol%) were synthesized successfully by solid-state reaction method. The phosphors retained the orthorhombic crystal structure of the host matrix without other impurity phases. FTIR results confirmed the formation of pyrophosphate groups in the phosphors. The surface states of the phosphors regarding Li–O, Na–O, P–O, and Dy–O bonds were identified by XPS analysis. With an excitation wavelength of 351 nm, the phosphor showed two broad bands in the blue and yellow regions, and the combination of these two bands produced near-white-light color coordinates (0.281, 0.338).

Acknowledgements

The author B. Deva Prasad Raju is highly thankful to the Department of Science and Technology of the Government of India for providing financial assistance to carry out this research work in the form of DST Fast Track Major Research Project; vide reference no: DST-SR/FTP/PS-198/2012; dated:14-02-2014. Dr. Shivanand Chaurasia is thankful to Dr S. M. Sharma, Director, Physics Group and Head, HP & SRPD Bhabha Atomic Research Centre, Mumbai for his kind support and fruit full discussions.

References

[1] K.-S. Sohn, I.W. Zeon, H. Chang, S.K. Lee, H.D. Park, Combinatorial search for new red phosphors of high efficiency at VUV excitation based on the YRO_4(R = As, Nb, P, V) System, Chem. Mater. 14 (2002) 2140–2148.
[2] T. Hashimoto, F. Wu, J.S. Speck, S. Nakamura, A GaN bulk crystal with improved structural quality grown by the ammonothermal method, Nat. Mater. 6 (2007) 568–571.
[3] A.J. Fernández-Carrión, M. Ocaña, J. García-Sevillano, E. Cantelar, A.I. Becerro, New Single-Phase, White-Light-Emitting Phosphors Based on δ-$Gd_2Si_2O_7$ for Solid-State Lighting, J. Phys. Chem. C 118 (2014) 18035–18043.
[4] Y.-D. Huh, J.-H. Shim, Y. Kim, Y.R. Doc, Optical Properties of Three-Band White Light Emitting Diodes, J. Electrochem. Soc. 150 (2003) H57–H60.
[5] D. Haranath, H. Chander, P. Sharma, S. Singh, Enhanced luminescence of $Y_3Al_5O_{12}:Ce^{3+}$ nanophosphor for white light-emitting diodes, Appl. Phys. Lett. 89 (2006) 173118.
[6] B. Han, P. Li, J. Zhang, J. Zhang, Y. Xue, H. Shi, The effect of Li^+ ions on the luminescent properties of a single-phase white light-emitting phosphor α-$Sr_2P_2O_7:Dy^{3+}$, Dalt. Trans. 44 (2015) 7854–7861.
[7] M. Shang, C. Li, J. Lin, How to produce white light in a single-phase host? Chem. Soc. Rev. 43 (2014) 1372–1386.
[8] Z. Zhou, F. Wang, S. Liu, K. Huang, Z. Li, S. Zeng, K. Jiang, A single-phase phosphor $Ba_3LiMgV_3O_{12}$: Eu^{3+} for white light-emitting diodes, J. Electrochem. Soc. 158 (2011) H1238.
[9] F. Liu, Q. Liu, Y. Fang, N. Zhang, B. Yang, G. Zhao, White light emission from $NaLa(PO_3)_4:Dy^{3+}$ single-phase phosphors for light-emitting diodes, Ceram. Int. 41 (2015) 1917–1920.
[10] F. Yang, Y. Liang, M. Liu, X. Li, X. Wu, N. Wang, $YAl_3(BO_3)_4:Tm^{3+}$, Dy^{3+}: A potential tunable single-phased white-emitting phosphors, Optik 124 (2013) 2004–2007.
[11] L. Jiang, R. Pang, D. Li, W. Sun, Y. Jia, H. Li, J. Fu, C. Li, S. Chang, Tri-chromatic white-light emission from a single-phase $Ca_9Sc(PO_4)_7:Eu^{2+},Tb^{3+},Mn^{2+}$ phosphor for LED applications, Dalt. Trans. 44 (2015) 17241–17250.
[12] J. Sun, Z. Lian, G. Shen, D. Shen, Blue–white–orange color-tunable luminescence of Ce^{3+}/Mn^{2+}-codoped $NaCaBO_3$via energy transfer: potential single-phase white-light-emitting phosphors, RSC Adv. 3 (2013) 18395.
[13] W.-R. Liu, C. Huang, C.-W. Yeh, J.-C. Tsai, Y.-C. Chiu, Y.-T. Yeh, R.-S. Liu, A study on the luminescence and energy transfer of single-phase and color-tunable

KCaY$(PO_4)_2$:Eu^{2+},Mn^{2+} phosphor for application in white-light LEDs, Inorg. Chem. 51 (2012) 9636–9641.
[14] Y. Liu, B. Lei, C. Shi, Luminescent properties of a white afterglow phosphor $CdSiO_3$:Dy^{3+}, Chem. Mater 17 (2005) 2108–2113.
[15] G.R. Dillip, S.J. Dhoble, L. Manoj, C. Madhukar Reddy, B. Deva Prasad Raju, A potential red emitting $K_4Ca(PO_4)_2$: Eu^{3+} phosphor for white light emitting diodes, J. Lumin 132 (2012) 3072–3076.
[16] I.M. Nagpure, S. Saha, S.J. Dhoble, Photoluminescence and thermoluminescence characterization of Eu^{3+}- and Dy^{3+} -activated $Ca_3(PO_4)_2$ phosphor, J. Lumin 129 (2009) 898–905.
[17] B. Liu, C. Shi, Z. Qi, Potential white-light long-lasting phosphor: Dy^{3+}-doped aluminate, Appl. Phys. Lett. 86 (2005) 191111.
[18] S.K. Gupta, M. Mohapatra, V. Natarajan, S.V. Godbole, Photoluminescence investigations of the near white light emitting perovskite ceramic $SrZrO_3$:Dy^{3+} Prepared Via Gel-Combustion Route, Int. J. Appl. Ceram. Technol. 10 (2013) 593–602.
[19] G.R. Dillip, S.J. Dhoble, B.D.P. Raju, Luminescence properties of $Na_3SrB_5O_{10}$:Dy^{3+} plate-like microstructures for solid state lighting applications, Opt. Mater 35 (2013) 2261–2266.
[20] S. Chemingui, M. Ferhi, K. Horchani-Naifer, M. Férid, Synthesis and luminescence characteristics of Dy^{3+} doped $KLa(PO_3)_4$, J. Lumin. 166 (2015) 82–87.
[21] K. Munirathnam, G.R. Dillip, B. Ramesh, S.W. Joo, B.D. Prasad Raju, Synthesis, photoluminescence and thermoluminescence properties of $LiNa_3P_2O_7$:Tb^{3+} green emitting phosphor, J. Phys. Chem. Solids 86 (2015) 170–176.
[22] Y. Shi, Y.W. Shilie Pan, Z. Yang, X. Dong, H. Wu, M. Zhang, J. Cao, Z. Zhou, Synthesis, crystal structures and optical properties of two congruent-meltingisotypic diphosphates: $LiM_3P_2O_7$ (M = Na, K), J. Solid State Chem. 197 (2013) 128–133.
[23] E.S. Shim, H.S. Kang, S.S. Pang, J.S. Kang, I. Yun, S.Y. Lee, Annealing effect on the structural and optical properties of ZnO thin film on InP, Mater. Sci. Eng. B 102 (2003) 366–369.
[24] M. Chen, Z.L. Pei, C. Sun, L.S. Wen, X. Wang, Surface characterization of transparent conductive oxide Al-doped ZnO films, J. Cryst. Growth 220 (2000) 254–262.
[25] D.-C. Li, T. Muta, L.-Q. Zhang, M. Yoshio, H. Noguchi, Effect of synthesis method on the electrochemical performance of $LiNi_{1/3}Mn_{1/3}Co_{1/3}O_2$, J. Power Sources 132 (2004) 150–155.
[26] R.D. Shannon, Revised effective ionic radii and systematic studies of interatomic distances in halides and chalcogenides, Acta Crystallogr. Sect. A 32 (1976) 751–767.
[27] G.R. Dillip, P. Mohan Kumar, B. Deva Prasad Raju, S.J. Dhoble, Synthesis and luminescence properties of a novel $Na_6CaP_2O_9$:Sm^{3+} phosphor, J. Lumin 134 (2013) 333–338.
[28] Y.Q. Jia, Radii and Effective Ionic Radii of the Rare Earth Ions, J. Solid State Chem. 187 (1991) 184–187.
[29] A. Zaafouri, M. Megdiche, M. Gargouri, AC conductivity and dielectric behavior in lithium and sodium diphosphate $LiNa_3P_2O_7$, J. Alloys Compd. 584 (2014) 152–158.
[30] H. Pfeiffer, P. Bosch, J.A. Odriozola, A. Lopez, J.A. Ascencio, S. Bulbulian, Sol-gel synthesis of Li – $ZrSiO_4$, J. Mater. Res. 4 (2000) 5–10.
[31] S.S. Pitale, I.M. Nagpure, V. Kumar, O.M. Ntwaeaborwa, J.J. Terblans, H.C. Swart, Investigations on the low voltage cathodoluminescence stability and surface chemical behaviour using Auger and X-ray photoelectron spectroscopy on $LiSrBO_3$:Sm^{3+} phosphor, Mater. Res. Bull. 46 (2011) 987–994.
[32] S.P. Kowalczyk, L. Ley, F.R. McFeely, R.A. Pollak, D.A. Shirley, X-Ray Photoemission from Sodium and Lithium, Phys. Rev. B 8 (1973) 3583–3585.
[33] A.M. Puziy, O.I. Poddubnaya, R.P. Socha, J. Gurgul, M. Wisniewski, XPS and NMR studies of phosphoric acid activated carbons, Carbon 46 (2008) 2113–2123.
[34] B. Ramesh, G. Devarajulu, B.D.P. Raju, G.B. Kumar, G.R. Dillip, A.N. Banerjee, S.W. Joo, Determination of strain, site occupancy, photoluminescent, and thermoluminescent-trapping parameters of Sm^{3+}-doped $NaSrB_5O_9$ microstructures, Ceram. Int. 42 (2016) 1234–1245.
[35] D. Barreca, A. Gasparotto, A. Milanov, E. Tondello, A. Devi, R.A. Fischer, Nanostructured Dy_2O_3 films: An XPS Investigation, Surf. Sci. Spectra 14 (2007) 52.
[36] K. Granath, M. Bodegård, L. Stolt, The effect of NaF on Cu(In,Ga)Se_2 thin film solar cells, Sol. Energy Mater. Sol. Cells 60 (2000) 279–293.
[37] A. Majjane, A. Chahine, M. Et-Tabirou, B. Echchahed, T.O. Do, P.M. Breen, X-ray photoelectron spectroscopy (XPS) and FTIR studies of vanadium barium phosphate glasses, Mater. Chem. Phys. 143 (2014) 779–787.
[38] V. Venckutė, J. Miškinis, V. Kazlauskienė, T. Šalkus, A. Dindune, Z. Kanepe, J. Ronis, A. Maneikis, M. Lelis, A. Kezionis, A.F. Orliuka, XRD, XPS, SEM/EDX and broadband impedance spectroscopy study of pyrophosphate ($LiFeP_2O_7$ and $Li_{0.9}Fe_{0.9}Ti_{0.1}P_2O_7$) ceramics, Phase Transit. 87 (2014) 438–451.
[39] G.R. Dillip, B. Ramesh, C.M. Reddy, K. Mallikarjuna, O. Ravi, S.J. Dhoble, S.W. Joo, B. Deva Prasad Raju, X-ray analysis and optical studies of Dy^{3+} doped $NaSrB_5O_9$ microstructures for white light generation, J. Alloys Compd. 615 (2014) 719–727.
[40] A. Watras, P.J. Dereń, R. Pązik, Luminescence properties and determination of optimal RE^{3+} (Sm^{3+}, Tb^{3+} and Dy^{3+}) doping levels in the KYP_2O_7 host lattice obtained by combustion synthesis, New J. Chem. 38 (2014) 5058–5068.
[41] G. Blasse, Energy transfer between inequivalent Eu^{2+} ions, J. Solid State Chem. 211 (1986) 207–211.
[42] Q. Xu, J. Sun, D. Cui, Q. Di, J. Zeng, Synthesis and luminescence properties of novel $Sr_3Gd(PO_4)_3$:Dy^{3+} phosphor, J. Lumin 158 (2015) 301–305.
[43] Z.-W. Zhang, X.-Y. Sun, L. Liu, Y. Peng, X. Shen, W.-G. Zhang, D.-J. Wang, Synthesis and luminescence properties of novel $LiSr_4(BO_3)_3$:Dy^{3+} phosphors, Ceram. Int. 39 (2013) 1723–1728.